

Inhibition of Acetylcholinesterase with Novel 1, 3, 4, Oxadiazole Derivatives: A Kinetic, *In Silico*, and *In Vitro* Approach

Farida Begum,¹ Muhammad Yousaf,¹ Sajid Iqbal, Nazif Ullah, Anwar Hussain, Momin Khan, Asaad Khalid,* Alanood S. Algarni, Ashraf N. Abdalla, Ajmal Khan,* Muhammad Arif Lodhi,* and Ahmed Al-Harrasi*



Cite This: *ACS Omega* 2023, 8, 46816–46829



Read Online

ACCESS |



Metrics & More

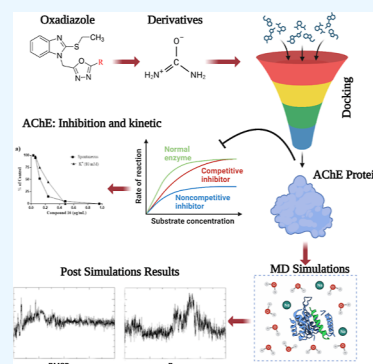


Article Recommendations



Supporting Information

ABSTRACT: Alzheimer's disease (AD) is a neurological disease that disturbs the memory, thinking skills, and behavior of the affected person. AD is a complex disease caused by the breakdown of acetylcholine *via* acetylcholinesterase (AChE). The present study aimed to assess the synthetic inhibitors of AChE that could be used to treat AD. For this purpose, synthetic compounds of oxadiazole derivatives (15–35) were evaluated and identified as promising inhibitors of AChE, exhibiting IC_{50} varying between 41.87 ± 0.67 and $1580.25 \pm 0.7 \mu\text{M}$. The kinetic parameters indicated that all the studied compounds bind to the allosteric site and decrease the efficiency of the AChE enzyme. *In silico* docking analysis showed that the majority of the compounds interact with the anionic subsite and Per-Arnt-Sim domain of AChE and are stabilized by various bonds including π – π and hydrogen bonding. The stability of the most potent compounds 16 and 17 with AChE interaction was confirmed by molecular dynamics simulations. Moreover, all compounds exhibited concentration-dependent calcium (Ca^{2+}) antagonistic and spasmolytic activities. Among the whole series of oxadiazole derivatives, compounds 16 and 17 displayed the highest activities on spontaneous and potassium (K^+)-induced contraction. Therefore, the AChE inhibitory potential, cytotoxicity safe profile, and Ca^{2+} antagonistic ability of these compounds make them potential therapeutic agents against AD and its associated problems in the future.



INTRODUCTION

The life-threatening implications of multifactorial disorders such as Alzheimer's disease (AD) pose a challenge for physicians as well as the scientific community.¹ The loss of cognitive function has been reported in various neurodegenerative diseases including AD.² It is a severe neurological disorder with a high mortality rate in the old age population.³ Recently, AD facts and Figures 2022 were published, which urge researchers to discover new therapeutic options with novel mechanisms to treat AD.⁴ Amyloid aggregation and impaired cholinergic transmission are the two commonly used therapeutic strategies for AD.⁵ Acetylcholinesterase (AChE) is responsible for acetylcholine (ACh) hydrolysis, which was reported to be negatively affecting intellectual capabilities.⁶ Several AChE inhibitors have been discovered in recent years that pave the way for a better treatment option for improving cognition in people suffering from AD.⁷ Nevertheless, they are unable to treat all the complications and fail to completely eradicate the disease.⁸ AChE has also been reported to be associated with increased levels of accumulation of amyloid-beta ($A\beta$) aggregates in AD.⁹ The $A\beta$ fibrils and oligomer aggregations and accumulation result into a disturbance in cell signaling, progressive neurotic injury, poor immunity, neuronal shortfalls, and loss of cognitive function.¹⁰ Deposition of $A\beta$

also causes brain damage by producing free radicals in mitochondria.¹¹

Over the past few decades, oxadiazole and its derivatives got researchers' attention due to its synthetic versatility and therapeutic potential. Oxadiazole's unique structural properties allowed researchers to find potent AChE inhibitors with a variety of different structures.¹² The versatile structure of 1,3,4-oxadiazole with various V, VI, and VII positions' substations exhibits both AChE inhibitory and antioxidant property structures.^{12–14} The core structure of oxadiazole is also responsible for pharmacological effects, including its antiviral, anti-inflammatory, antibacterial, antimalarial, analgesic, anti-depressant, and anticancer properties.¹⁵

Herein, a novel series of oxadiazole compounds (15–35) were assessed for their potential to prevent the catalytic reaction of AChE. Moreover, binding interactions and stability of these compounds were determined using kinetics study,

Received: August 24, 2023

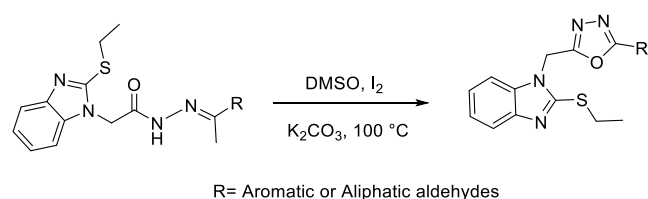
Accepted: September 20, 2023

Published: November 27, 2023



molecular docking, and molecular dynamics (MD) simulation (Scheme 1).

Scheme 1. Schematic Representation of 1, 3, 4-Oxadiazole Derivatives (15–35) Synthesis



MATERIALS AND METHODS

In the current study, all chemical reagents utilized were of analytical grade: AChE EC 3.1.1.7 (Cat. no. C3389-2KU), ACh iodide (Cat. no. A7000-25G), DTNB (5-dithiobis 2-nitrobenzoic acid) (Cat. no. D8130-10G), and galanthamine (Cat. no. 69353-21-5) (MO, USA). Sodium phosphate monobasic dehydrate buffer (Cat. no. 1342-35-0), di-Sodium hydrogen phosphate (Cat. no. 558-79-4), and ethanol (Cat. no. 64-17-5) were purchased from Sigma-Aldrich. All analogues of oxadiazole derivatives (15–35) were synthesized and characterized by using different spectroscopic techniques ^1H and ^{13}C nuclear magnetic resonance (NMR). Electron impact mass spectra were recorded on MAT 711 (70 eV) spectrometers, and data were tabulated as m/z ratios. A Fisher John melting point device was used to know the melting points (mp) of the synthesized compounds.

^1H NMR and ^{13}C NMR Study of Compounds 15–35. 2-((2-(Ethylthio)-1H-benzo[d]imidazole-1-yl)methyl)-5-(4-fluorophenyl)-1,3,4-oxadiazole (15). Molecular Formula: $\text{C}_{18}\text{H}_{15}\text{FN}_4\text{O}_5$. Yield: 0.29 g (83%); mp: 125–127 °C; ^1H NMR (400 MHz, $\text{DMSO}-d_6$): δ 7.92 (dd, $J = 8.4, 5.0$ Hz, 2H), 7.57 (dd, $J = 7.5, 1.1$ Hz, 1H), 7.45 (dd, $J = 7.5, 1.1$ Hz, 1H), 7.33–7.25 (m, 3H), 7.21 (td, $J = 7.5, 1.4$ Hz, 1H), 5.29 (s, 2H), 3.14 (q, $J = 7.2$ Hz, 2H), 1.37 (t, $J = 7.1$ Hz, 3H). ^{13}C NMR (100 MHz, $\text{DMSO}-d_6$): δ 163.37, 162.44, 160.34, 157.19, 146.75, 138.39, 127.67, 127.24, 126.67, 121.76, 120.41, 118.71, 116.53, 115.43, 111.72, 43.46, 28.91, 17.76; EI-MS m/z (% relative abundance): 354 (M^+ , 62), 294 (100), 164 (46), 117 (68).

2-((2-(Ethylthio)-1H-benzo[d]imidazole-1-yl)methyl)-5-heptyl-1,3,4-oxadiazole (16). Molecular Formula: $\text{C}_{19}\text{H}_{26}\text{N}_4\text{O}_5$. Yield: 0.23 g (85%); mp: 163–165 °C; ^1H NMR (400 MHz, $\text{DMSO}-d_6$): δ 7.56 (dd, $J = 7.8, 1.3$ Hz, 1H), 7.45 (dd, $J = 7.9, 1.3$ Hz, 1H), 7.27 (td, $J = 7.6, 1.4$ Hz, 1H), 7.21 (td, $J = 7.5, 1.4$ Hz, 1H), 5.27 (s, 2H), 3.16 (q, $J = 7.0$ Hz, 2H), 2.74 (t, $J = 6.4$ Hz, 2H), 1.90 (q, $J = 6.6$ Hz, 2H), 1.38–1.27 (m, 11H), 0.89 (m, 3H). ^{13}C NMR (100 MHz, $\text{DMSO}-d_6$): δ 167.53, 164.38, 159.13, 148.35, 138.39, 128.34, 125.36, 121.81, 113.72, 43.54, 37.84, 31.26, 28.59, 27.86, 26.54, 25.97, 21.68, 13.37, 12.68; EI-MS m/z (% relative abundance): 358 (M^+ , 31), 298 (100), 167 (39), 133 (51).

2-((2-(Ethylthio)-1H-benzo[d]imidazole-1-yl)methyl)-5-(furan-2-yl)-1,3,4-oxadiazole (17). Molecular Formula: $\text{C}_{16}\text{H}_{14}\text{N}_4\text{O}_2\text{S}$. Yield: 0.21 g (81%); mp: 105–107 °C; ^1H NMR (400 MHz, $\text{DMSO}-d_6$): δ 7.70 (dd, $J = 6.5, 1.3$ Hz, 1H), 7.56 (dd, $J = 6.9, 1.8$ Hz, 1H), 7.44 (dd, $J = 6.9, 1.8$ Hz, 1H), 7.30 (dd, $J = 7.9, 1.5$ Hz, 1H), 7.31–7.25 (m, 2H), 6.57 (dd, $J = 7.8, 1.5$ Hz, 1H), 5.26 (s, 2H), 3.19 (q, $J = 7.2$ Hz, 2H), 1.34

(t, $J = 7.2$ Hz, 3H). ^{13}C NMR (100 MHz, $\text{DMSO}-d_6$): δ 160.68, 160.62, 157.83, 146.86, 144.71, 138.69, 136.24, 127.75, 123.51, 121.32, 118.23, 116.64, 108.54, 44.36, 27.91, 17.81; EI-MS m/z (% relative abundance): 326 (M^+ , 100), 266 (88), 146 (47), 135 (71).

2-((2-(Ethylthio)-1H-benzo[d]imidazole-1-yl)methyl)-1,3,4-oxadiazol-2-yl)-6-methoxyphenol (18). Molecular Formula: $\text{C}_{19}\text{H}_{18}\text{N}_4\text{O}_3\text{S}$. Yield: 0.21 g (81%); mp: 131–132 °C; ^1H NMR (400 MHz, $\text{DMSO}-d_6$): δ 9.06 (s, 1H), 7.70 (dd, $J = 7.7, 1.3$ Hz, 1H), 7.56 (dd, $J = 7.7, 1.4$ Hz, 1H), 7.45 (dd, $J = 7.7, 1.4$ Hz, 1H), 7.30–7.18 (m, 2H), 7.00 (t, $J = 7.8$ Hz, 1H), 6.91 (dd, $J = 7.9, 1.3$ Hz, 1H), 5.37 (s, 2H), 3.89 (s, 3H), 3.19 (q, $J = 7.3$ Hz, 2H), 1.34 (t, $J = 7.3$ Hz, 3H). ^{13}C NMR (100 MHz, $\text{DMSO}-d_6$): δ 160.35, 158.39, 153.41, 148.47, 147.23, 142.42, 136.16, 126.36, 121.27, 120.14, 118.20, 116.54, 115.33, 112.82, 107.25, 59.59, 43.28, 29.31, 17.61; EI-MS m/z (% relative abundance): 382 (M^+ , 38), 322 (100), 191 (62), 146 (53).

2-Ethoxy-6-(5-((2-(ethylthio)-1H-benzo[d]imidazole-1-yl)methyl)-1,3,4-oxadiazol-2-yl)phenol (19). Molecular Formula: $\text{C}_{20}\text{H}_{20}\text{N}_4\text{O}_3\text{S}$. Yield: 0.23 g (89%); mp: 135–136 °C; ^1H NMR (400 MHz, $\text{DMSO}-d_6$): δ 9.09 (s, 1H), 7.69 (dd, $J = 7.8, 1.2$ Hz, 1H), 7.56 (dd, $J = 7.6, 1.5$ Hz, 1H), 7.45 (dd, $J = 7.7, 1.4$ Hz, 1H), 7.22–7.13 (m, 2H), 6.98 (t, $J = 7.8$ Hz, 1H), 6.87 (dd, $J = 7.8, 1.2$ Hz, 1H), 5.33 (s, 2H), 4.13 (q, $J = 6.9$ Hz, 2H), 3.12 (q, $J = 7.4$ Hz, 2H), 1.41 (t, $J = 6.9$ Hz, 3H), 1.39 (t, $J = 7.3$ Hz, 3H). ^{13}C NMR (100 MHz, $\text{DMSO}-d_6$): δ 163.76, 159.45, 155.23, 151.86, 149.22, 143.26, 138.38, 127.47, 123.32, 121.14, 120.27, 119.92, 116.49, 111.40, 108.45, 67.37, 48.21, 29.41, 19.23, 15.91; EI-MS m/z (% relative abundance): 396 (M^+ , 93), 336 (100), 205 (68), 131 (33).

2-((2-(Ethylthio)-1H-benzo[d]imidazole-1-yl)methyl)-5-(4-methoxyphenyl)-1,3,4-oxadiazole (20). Molecular Formula: $\text{C}_{19}\text{H}_{18}\text{N}_4\text{O}_2\text{S}$. Yield: 0.25 g (81%); mp: 112–114 °C; ^1H NMR (400 MHz, $\text{DMSO}-d_6$): δ 7.74 (dd, $J = 7.5, 1.7$ Hz, 1H), 7.57 (dd, $J = 7.5, 1.2$ Hz, 1H), 7.45 (dd, $J = 7.5, 1.2$ Hz, 1H), 7.32–7.21 (m, 4H), 7.00 (dd, $J = 7.2, 1.8$ Hz, 1H), 5.32 (s, 2H), 3.91 (s, 3H), 3.18 (q, $J = 7.2$ Hz, 2H), 1.39 (t, $J = 7.2$ Hz, 3H). ^{13}C NMR (100 MHz, $\text{DMSO}-d_6$): δ 164.86, 160.55, 157.30, 153.44, 147.67, 139.36, 136.56, 129.47, 126.96, 124.67, 123.34, 121.72, 118.56, 116.59, 113.72, 59.94, 48.34, 28.51, 19.34; EI-MS m/z (% relative abundance): 366 (M^+ , 100), 336 (94), 306 (57), 175 (48), 131 (46).

2-((2-(Ethylthio)-1H-benzo[d]imidazole-1-yl)methyl)-5-(2-methoxyphenyl)-1,3,4-oxadiazole (21). Molecular Formula: $\text{C}_{19}\text{H}_{18}\text{N}_4\text{O}_2\text{S}$. Yield: 0.26 g (87%); mp: 110–112 °C; ^1H NMR (400 MHz, $\text{DMSO}-d_6$): δ 7.77 (dd, $J = 7.8, 1.4$ Hz, 1H), 7.60–7.46 (m, 2H), 7.36–7.17 (m, 4H), 7.05 (dd, $J = 7.5, 1.5$ Hz, 1H), 5.25 (s, 2H), 3.87 (s, 3H), 3.06 (q, $J = 7.3$ Hz, 2H), 1.37 (t, $J = 7.3$ Hz, 3H). ^{13}C NMR (100 MHz, $\text{DMSO}-d_6$): δ 163.36, 162.38, 159.43, 155.81, 147.48, 138.21, 133.54, 129.89, 124.10, 122.30, 120.97, 118.31, 116.23, 113.89, 108.34, 57.56, 43.34, 28.91, 17.23; EI-MS m/z (% relative abundance): 366 (M^+ , 45), 336 (100), 306 (75), 175 (32), 131 (66).

2-((2-(Ethylthio)-1H-benzo[d]imidazole-1-yl)methyl)-5-(5-methylfuran-2-yl)-1,3,4-oxadiazole (22). Molecular Formula: $\text{C}_{17}\text{H}_{16}\text{N}_4\text{O}_2\text{S}$. Yield: 0.22 g (80%); mp: 108–110 °C; ^1H NMR (400 MHz, $\text{DMSO}-d_6$): δ 7.58–7.55 (dd, $J = 7.7, 1.2$ Hz, 1H), 7.43 (dd, $J = 7.7, 1.2$ Hz, 1H), 7.21–7.11 (m, 2H), 7.17 (d, $J = 8.5$ Hz, 1H), 6.28 (dd, $J = 8.4, 0.7$ Hz, 1H), 5.37 (s, 2H), 3.21 (q, $J = 7.2$ Hz, 2H), 2.37 (s, 3H), 1.32 (t, $J = 7.1$ Hz, 3H). ^{13}C NMR (100 MHz, $\text{DMSO}-d_6$): δ 161.70, 161.54, 157.43, 153.33, 145.55, 142.54, 135.64, 126.88, 123.87, 117.31,

113.53, 110.53, 105.56, 41.34, 24.41, 15.41, 12.47; EI-MS m/z (% relative abundance): 340 (M^+ , 100), 304 (45), 167 (51), 131 (78).

2-(2-Chlorophenyl)-5-((2-(ethylthio)-1H-benzo[d]imidazole-1-yl)methyl)-1,3,4-oxadiazole (23). Molecular Formula: $C_{18}H_{15}ClN_4OS$. Yield: 0.14 g (71%); mp: 122–124 °C; 1H NMR (400 MHz, DMSO- d_6): δ 7.63 (dd, $J = 7.7, 1.3$ Hz, 1H), 7.60–7.53 (m, 2H), 7.50–7.40 (m, 2H), 7.34 (td, $J = 7.6, 1.5$ Hz, 1H), 7.27–7.19 (m, 2H), 5.34 (s, 2H), 3.19 (q, $J = 7.3$ Hz, 2H), 1.33 (t, $J = 7.2$ Hz, 3H). ^{13}C NMR (100 MHz, DMSO- d_6): δ 162.78, 161.89, 157.56, 147.88, 135.78, 132.95, 132.30, 128.34, 123.32, 122.22, 121.94, 121.27, 120.35, 117.31, 108.77, 43.12, 28.33, 19.32; EI-MS m/z (% relative abundance): 370 (M^+ , 22), 334 (100), 217 (21), and 131 (52).

2-(3,4-Dimethoxyphenyl)-5-((2-(ethylthio)-1H-benzo[d]imidazole-1-yl)methyl)-1,3,4-oxadiazole (24). Molecular Formula: $C_{20}H_{20}N_4O_3S$. Yield: 0.24 g (84%); mp: 109–111 °C; 1H NMR (400 MHz, DMSO- d_6): δ 7.74 (dd, $J = 7.5, 1.7$ Hz, 1H), 7.57 (dd, $J = 7.5, 1.2$ Hz, 1H), 7.45 (dd, $J = 7.5, 1.2$ Hz, 1H), 7.32–7.21 (m, 4H), 7.00 (dd, $J = 7.2, 1.8$ Hz, 1H), 5.32 (s, 2H), 3.91 (s, 3H), 3.18 (q, $J = 7.2$ Hz, 2H), 1.39 (t, $J = 7.2$ Hz, 3H). ^{13}C NMR (100 MHz, DMSO- d_6): δ 164.86, 160.55, 157.30, 153.44, 147.67, 139.36, 136.56, 129.47, 126.96, 124.67, 123.34, 121.72, 118.56, 116.59, 113.72, 59.94, 48.34, 28.51, 19.34; EI-MS m/z (% relative abundance): 396 (M^+ , 100), 321 (56), 197 (77), 131 (45).

2-(4-Chlorophenyl)-5-((2-(ethylthio)-1H-benzo[d]imidazole-1-yl)methyl)-1,3,4-oxadiazole (25). Molecular Formula: $C_{18}H_{15}ClN_4OS$. Yield: 0.16 g (72%); mp: 123–125 °C; 1H NMR (400 MHz, DMSO- d_6): δ 8.05 (d, $J = 8.4$ Hz, 2H), 7.57 (dd, $J = 7.8, 1.2$ Hz, 1H), 7.50–7.41 (m, 3H), 7.34–7.27 (m, 2H), 5.27 (s, 2H), 3.16 (q, $J = 7.0$ Hz, 2H), 1.38 (t, $J = 7.0$ Hz, 3H). ^{13}C NMR (100 MHz, DMSO- d_6): δ 166.26, 163.77, 155.45, 143.43, 138.11, 136.22, 128.33, 126.45, 125.22, 122.23, 121.35, 116.88, 106.22, 47.32, 27.25, 16.65; EI-MS m/z (% relative abundance): 370 (M^+ , 32), 335 (100), 156 (34), 131 (75).

4-(5-((2-(Ethylthio)-1H-benzo[d]imidazole-1-yl)methyl)-1,3,4-oxadiazol-2-yl)phenol (26). Molecular Formula: $C_{18}H_{16}N_4O_2S$. Yield: 0.21 g (79%); mp: 120–122 °C; 1H NMR (400 MHz, DMSO- d_6): δ 8.32 (s, 1H), 7.98 (d, $J = 8.4$ Hz, 2H), 7.57 (dd, $J = 7.5, 1.0$ Hz, 1H), 7.45 (dd, $J = 7.5, 1.0$ Hz, 1H), 7.30–7.20 (m, 2H), 7.00 (d, $J = 8.4$ Hz, 2H), 5.23 (s, 2H), 3.14 (q, $J = 7.3$ Hz, 2H), 1.35 (t, $J = 7.3$ Hz, 3H). ^{13}C NMR (100 MHz, DMSO- d_6): δ 166.42, 163.66, 158.61, 155.28, 146.66, 139.23, 126.45, 125.51, 123.46, 118.71, 118.41, 113.32, 110.72, 43.43, 25.41, 19.78; EI-MS m/z (% relative abundance): 352 (M^+ , 100), 305 (67), 136 (64), 131 (36).

2-((2-(Ethylthio)-1H-benzo[d]imidazole-1-yl)methyl)-5-(3,4,5-trimethoxyphenyl)-1,3,4-oxadiazole (27). Molecular Formula: $C_{21}H_{22}N_4O_4S$. Yield: 0.23 g (82%); mp: 106–108 °C; 1H NMR (400 MHz, DMSO- d_6): δ 7.56 (dd, $J = 7.7, 1.2$ Hz, 1H), 7.45 (dd, $J = 7.7, 1.2$ Hz, 1H), 7.24 (td, $J = 7.4, 1.6$ Hz, 1H), 7.21 (s, 3H), 5.28 (s, 2H), 3.86 (s, 6H), 3.80 (s, 3H), 3.14 (q, $J = 7.2$ Hz, 2H), 1.33 (t, $J = 7.2$ Hz, 3H). ^{13}C NMR (100 MHz, DMSO- d_6): δ 163.24, 160.47, 154.93, 154.76, 143.47, 140.83, 133.75, 125.68, 122.72, 118.33, 117.84, 112.52, 107.30, 64.33, 57.25, 45.13, 27.41, 15.53; EI-MS m/z (% relative abundance): 426 (M^+ , 47), 396 (37), 366 (87), 336 (100).

2-((2-(Ethylthio)-1H-benzo[d]imidazole-1-yl)methyl)-5-(4-nitrophenyl)-1,3,4-oxadiazole (28). Molecular Formula: $C_{18}H_{15}N_5O_3S$. Yield: 0.27 g (85%); mp: 1118–119 °C; 1H

NMR (400 MHz, DMSO- d_6): δ 8.31 (d, $J = 8.5$ Hz, 2H), 8.21 (d, $J = 8.5$ Hz, 2H), 7.57 (dd, $J = 7.5, 1.2$ Hz, 1H), 7.44 (dd, $J = 7.7, 1.4$ Hz, 1H), 7.32–7.23 (m, 2H), 5.33 (s, 2H), 3.12 (q, $J = 7.2$ Hz, 2H), 1.39 (t, $J = 7.2$ Hz, 3H). ^{13}C NMR (100 MHz, DMSO- d_6): δ 166.21, 164.33, 158.11, 148.47, 146.45, 138.45, 128.19, 127.62, 124.46, 123.38, 122.46, 120.43, 110.75, 42.34, 25.45, 15.33; EI-MS m/z (% relative abundance): 381 (M^+ , 100), 336 (47), 177 (54), 145 (39).

2-((2-(Ethylthio)-1H-benzo[d]imidazole-1-yl)methyl)-5-(4-fluoro-3-methoxyphenyl)-1,3,4-oxadiazole (29). Molecular Formula: $C_{19}H_{17}FN_4O_2S$. Yield: 0.20 g (81%); mp: 115–117 °C; 1H NMR (400 MHz, DMSO- d_6): δ 7.71 (ddd, $J = 8.3, 5.0, 1.8$ Hz, 1H), 7.57 (dd, $J = 7.5, 1.2$ Hz, 1H), 7.44 (dd, $J = 7.7, 1.4$ Hz, 1H), 7.23–7.17 (m, 4H), 5.23 (s, 2H), 3.91 (s, 3H), 3.14 (q, $J = 7.3$ Hz, 2H), 1.35 (t, $J = 7.2$ Hz, 3H). ^{13}C NMR (100 MHz, DMSO- d_6): δ 163.32, 155.728, 153.76, 152.76, 148.07, 145.27, 136.86, 126.76, 123.94, 120.24, 116.87, 114.31, 111.53, 108.75, 56.62, 56.46, 43.46, 25.31, 15.316; EI-MS m/z (% relative abundance): 384 (M^+ , 38), 339 (100), 183 (47), 131 (40).

4-(5-((2-(Ethylthio)-1H-benzo[d]imidazole-1-yl)methyl)-1,3,4-oxadiazol-2-yl)benzene-1,3-diol (30). Molecular Formula: $C_{18}H_{16}N_4O_3S$. Yield: 0.19 g (70%); mp: 125–126 °C; 1H NMR (400 MHz, DMSO- d_6): δ 9.73 (s, 1H), 9.03 (s, 1H), 7.58 (dd, $J = 7.4, 1.1$ Hz, 1H), 7.45 (dd, $J = 7.4, 1.1$ Hz, 1H), 7.39 (d, $J = 8.5$ Hz, 1H), 7.34–7.25 (m, 2H), 6.55 (dd, $J = 8.4, 2.4$ Hz, 1H), 6.43 (d, $J = 2.3$ Hz, 1H), 5.32 (s, 2H), 3.21 (q, $J = 7.2$ Hz, 2H), 1.40 (t, $J = 7.2$ Hz, 3H). ^{13}C NMR (100 MHz, DMSO- d_6): δ 165.46, 162.45, 160.22, 158.83, 153.41, 146.55, 138.46, 128.25, 125.96, 121.84, 117.37, 109.75, 109.62, 105.94, 101.09, 42.28, 27.51, 13.65; EI-MS m/z (% relative abundance): 368 (M^+ , 100), 339 (100), 183 (31), 131 (56).

2-(5-((2-(Ethylthio)-1H-benzo[d]imidazole-1-yl)methyl)-1,3,4-oxadiazol-2-yl)phenol (31). Molecular Formula: $C_{18}H_{16}N_4O_2S$. Yield: 0.27 g (79%); mp: 121–122 °C; 1H NMR (400 MHz, DMSO- d_6): δ 9.13 (s, 1H), 7.60–7.51 (m, 2H), 7.44 (dd, $J = 7.5, 1.4$ Hz, 1H), 7.25–7.13 (m, 3H), 7.04 (td, $J = 7.7, 1.5$ Hz, 1H), 6.97 (dd, $J = 7.9, 1.5$ Hz, 1H), 5.37 (s, 2H), 3.12 (q, $J = 7.3$ Hz, 2H), 1.33 (t, $J = 7.2$ Hz, 3H). ^{13}C NMR (100 MHz, DMSO- d_6): δ 163.51, 162.35, 158.36, 156.45, 148.32, 139.29, 135.23, 127.45, 125.27, 124.26, 122.12, 117.31, 116.46, 112.96, 111.42, 49.28, 27.38, 12.63; EI-MS m/z (% relative abundance): 352 (M^+ , 28), 335 (100), 163 (71), 131 (38).

3-(5-((2-(Ethylthio)-1H-benzo[d]imidazole-1-yl)methyl)-1,3,4-oxadiazol-2-yl)phenol (32). Molecular Formula: $C_{18}H_{16}N_4O_2S$. Yield: 0.25 g (77%); mp: 140–141 °C; 1H NMR (400 MHz, DMSO- d_6): δ 9.43 (s, 1H), 7.57 (dd, $J = 7.9, 1.2$ Hz, 1H), 7.50 (dd, $J = 7.9, 1.2$ Hz, 1H), 7.45 (dd, $J = 7.9, 1.3$ Hz, 1H), 7.29–7.21 (m, 3H), 6.98 (s, 1H), 6.89 (dd, $J = 7.9, 1.2$ Hz, 1H), 5.25 (s, 2H), 3.16 (q, $J = 7.1$ Hz, 2H), 1.38 (t, $J = 7.1$ Hz, 3H). ^{13}C NMR (100 MHz, DMSO- d_6): δ 167.54, 163.54, 157.65, 155.36, 148.35, 139.32, 133.25, 126.53, 125.13, 123.67, 121.02, 118.81, 118.11, 113.76, 110.67, 41.45, 29.51, 19.84; EI-MS m/z (% relative abundance): 352 (M^+ , 39), 335 (100), 163 (54), 131 (78).

3-(5-((2-(Ethylthio)-1H-benzo[d]imidazole-1-yl)methyl)-1,3,4-oxadiazol-2-yl)benzene-1,2-diol (33). Molecular Formula: $C_{18}H_{16}N_4O_3S$. Yield: 0.21 g (73%); mp: 165–167 °C; 1H NMR (400 MHz, DMSO- d_6): δ 8.90 (s, 1H), 8.83 (s, 1H), 7.68 (dd, $J = 7.8, 1.2$ Hz, 1H), 7.57 (dd, $J = 7.4, 1.1$ Hz, 1H), 7.45 (dd, $J = 7.4, 1.1$ Hz, 1H), 7.33–7.24 (m, 2H), 7.00 (t, $J = 7.8$ Hz, 1H), 6.91 (dd, $J = 7.8, 1.2$ Hz, 1H), 5.26 (s, 2H), 3.13

(q, $J = 7.3$ Hz, 2H), 1.35 (t, $J = 7.3$ Hz, 3H). ^{13}C NMR (100 MHz, DMSO- d_6): δ 163.29, 162.49, 156.71, 149.56, 148.67, 146.45, 139.86, 129.06, 124.38, 122.85, 121.79, 118.45, 117.32, 113.57, 108.56, 46.56, 28.96, 17.67; EI-MS m/z (% relative abundance): 368 (M^+ , 59), 351 (75), 334 (100), 131 (18).

2-((2-(Ethylthio)-1H-benzo[d]imidazole-1-yl)methyl)-5-(*p*-tolyl)-1,3,4-oxadiazole (34). *Molecular Formula*: $\text{C}_{19}\text{H}_{18}\text{N}_4\text{O}_5$. Yield: 0.26 g (83%); mp: 105–107 °C; ^1H NMR (400 MHz, DMSO- d_6): δ 7.97 (d, $J = 8.6$ Hz, 2H), 7.57 (dd, $J = 7.6, 1.7$ Hz, 1H), 7.45 (dd, $J = 7.6, 1.6$ Hz, 1H), 7.34 (d, $J = 7.9$ Hz, 2H), 7.24 (m, 2H), 5.27 (s, 2H), 3.21 (q, $J = 7.2$ Hz, 2H), 2.43 (s, 3H), 1.33 (t, $J = 7.2$ Hz, 3H). ^{13}C NMR (100 MHz, DMSO- d_6): δ 165.34, 163.36, 157.18, 147.65, 143.54, 138.39, 133.12, 129.69, 127.38, 123.56, 122.79, 117.81, 108.42, 43.16, 27.41, 23.61, 16.78; EI-MS m/z (% relative abundance): 350 (M^+ , 37), 335 (100), 264 (35), 131 (73).

N,N-Diethyl-4-(5-((2-(ethylthio)-1H-benzo[d]imidazole-1-yl)methyl)-1,3,4-oxadiazol-2-yl)aniline (35). *Molecular Formula*: $\text{C}_{22}\text{H}_{25}\text{N}_5\text{O}_5$. Yield: 0.22 g (88%); mp: 131–133 °C; ^1H NMR (400 MHz, DMSO- d_6): δ 7.56 (dd, $J = 7.0, 2.2$ Hz, 1H), 7.52 (d, $J = 8.6$ Hz, 2H), 7.44 (dd, $J = 7.0, 1.8$ Hz, 1H), 7.26–7.16 (m, 2H), 6.80 (d, $J = 8.5$ Hz, 2H), 5.38 (s, 2H), 3.32 (q, $J = 7.2$ Hz, 4H), 3.15 (q, $J = 7.2$ Hz, 2H), 1.39 (t, $J = 7.2$ Hz, 3H), 1.23 (t, $J = 7.2$ Hz, 6H). ^{13}C NMR (100 MHz, DMSO- d_6): δ 162.90, 160.97, 153.96, 148.24, 145.37, 139.78, 128.30, 125.72, 122.06, 118.32, 116.24, 113.93, 107.45, 49.73, 46.34, 24.41, 18.21, 13.95; EI-MS m/z (% relative abundance): 307 (M^+ , 61), 351 (100), 241 (31), 131 (21).

AChE Inhibition Assay. The *in vitro* AChE inhibitory assay was determined as described previously with a minor modification using a 96-well plate reader (Molecular Devices, CA, USA).¹⁶ Initially, 140 μL of 100 mM (pH 8) sodium phosphate buffer (PBS), 10 μL (0.25 mM) of DTNB, 20 μL of AChE, and 0.5 mM of test compounds dissolved in 20 μL of ethanol were mixed and incubated for 15–20 min at 25 °C. Finally, 10 μL of 0.4 mM substrate (ACh) was added and incubated for 5 min at the same temperature. After the addition of the substrate, it was hydrolyzed by AChE in the presence of DTNB; as a result, 5-thio-2-nitrobenzoate anion (yellow color) was synthesized, which indicates that completion of the reaction optical density was measured at 412 nm. The FDA-approved AD drug Galanthamine was used as a standard drug. All experiments were carried out in triplicate and analyzed using SoftMax Pro6.3 (Molecular Devices, CA, USA).

Percent (%) inhibition was determined as

$$\frac{100 - \text{O. D. test well}}{\text{O. D. control}} \times 100$$

Enzyme Kinetics. The IC_{50} of test compounds was calculated at different concentrations using EZ-Fit EK (Perrella Scientific Inc., Amherst, USA).

Enzyme–substrate is the AChE and ACh complex, whereas P represents the product. The dissociation constant (K_i) values were estimated by the Lineweaver–Burk plot, Dixon plots, and their secondary replots.¹⁷

The kinetic constants K_m , $K_{m'}$, and V_{max} were calculated from Lineweaver–Burk and Dixon plots using a linear regression equation. K_i values were graphically determined using Dixon and Lineweaver–Burk plots.

Statistical Analysis. Graphs were plotted using Graft software.¹⁸ The linear regression equation was used to

determine the correlation coefficient, intercepts, slopes, and standard error values by the same software.

Docking of AChE and the Ligand. In order to find the binding interactions between ligands and AChE, docking was performed using the MOE-Dock module implanted in a molecular operating environment (MOE) (<https://www.chemcomp.com/Products.htm>). The 3D crystal structure of hAChE (PDB code 4EY6) at a resolution of 2.40 Å was retrieved from the protein data bank (PDB) (www.rcsb.org). Before docking analysis, 4EY6 was prepared by the Play molecule to complete the chain, add hydrogen atoms, and correct the bonds.¹⁹ All additional crystallized water molecules such as H_2O were removed, H atoms were added by 3D protonation, and energy was minimized using the MOE energy minimization algorithm.

3D structures of the new oxadiazole compounds were generated in the MOE molecular building program. After 3D protonation, minimization of energy (0.05 gradient) was performed by using MMFP94x force fields. Using the default parameters of the MOE-Dock program, all tested compounds were docked in the active site of AChE. Ten conformations were produced, and the top-rank conformations on the basis of docking score were selected for further *in silico* study. Before molecular docking, our docking protocol was confirmed by the redocking of a cocrystallized ligand of AChE (Figure S1).

MD Simulations. Top-ranked conformations of complexes of compound 19 and 21 with AChE were selected, and MD simulation was performed by employing the GROMACS 5.1 package.²⁰ The Pdb 2gm module in the Gromacs package was used to generate a protein–ligand complex. Protein parametrization and topology were generated using the OPLS-AA/L force field,²¹ and ligand topologies were generated by the Swissparam online Web server (<https://www.swissparam.ch/>). Each complex was solvated in a cubic box having dimensions of 10 × 10 × 10 surrounding approximately 33,437 TiP3P water molecules. Finally, 9 sodium ions were added to neutralize the enzyme–ligand complex. Energy minimization was performed through the steepest descent algorithm with position restraint until the maximal force 10 kJ/mol,²² removing the error in the atomic position and structural differences like bond length, bond angle, and the structural clashes between the ions, water molecule position, and protein complex.²³ Equilibration of the solvent around the protein was conducted in 2 phases; equilibration under the NVT ensemble and then NPT ensemble was used. Both NVT and NPT would run 50,000 steps at 300 K temperature and 1 bar pressure for 0.1 ns. Subsequently, each complex was subjected to MD simulation for 10,000,000 ps at 300,000 atmospheric NPT ensemble pressure and periodic boundary conditions for 0.002 ps using a leapfrog algorithm. LINCS algorithm was utilized to confine all hydrogen bonds during the whole process.²⁴ However, the Particle Mesh Ewald module with a 0.16 Å Fourier grid spacing was functionalized.²⁵

Ethics Approval and Consent to Participate. The experimental procedures on animals were approved by the Institutional Ethical Committee of Abdul Wali Khan University Mardan (AWKUM) (ethical approval ID: AWKUM/pharm-19).

Spasmolytic Calcium Antagonistic Activities. The spasmolytic antagonistic activity of oxadiazole compounds (15–35) was evaluated using rabbit jejunum by spontaneous contraction.²⁶ Local breed Rabbits were kindly provided by Agha Khan University, Pakistan. The standard experiment was

performed as described earlier.²⁶ Calcium antagonistic activity was also performed to confirm the capacity of the oxadiazole compounds (15–35) to relax the 80 mM K⁺-induced contraction.

Cytotoxicity Activity. Cytotoxicity was determined by using a human neutrophil viability assay. The heparinized fresh blood of healthy volunteers was obtained from a nearby blood bank and the required cells (neutrophils) were separated as described previously.²⁶ Human neutrophil isolation has been described elsewhere.²⁶ The neutrophil (1×10^7) was incubated for 30 min subsequently; 0.2 mM WAST-1 (Dojindo Laboratories, Japan) was added and incubated at 37 °C for 3 h. The O.D. was estimated at a 450 nm wavelength by utilizing a microplate reader (Spectra-MAX, CA, USA). The absorbance is the average of 5 experimental replicates. The viability percentage was determined as follows.

$$\text{viability \%} = \left[\left(\frac{\text{O. D. of compound} \times 100}{\text{O. D. of control}} \right) - 100 \right] - 100$$

RESULTS AND DISCUSSION

Chemistry. Synthesis of 1, 3, 4-oxadiazole derivatives was carried out by dissolving 1.0 mmol acyl hydrazone derivatives in 5 mL of dimethyl sulfoxide (DMSO) and then adding potassium carbonate (3 mmol) and the cyclizing agent, i.e., 1.2 mmol iodine, respectively. The entire mixture was continuously agitated in a water bath at 100 °C until complete product formation and was observed by using thin-layer chromatography (10–12 h). After cooling to ambient temperature, the reaction mixture was repeatedly treated with 5% sodium thiosulfate (Na₂S₂O₃) solution (10 mL) until the color of the mixture changed from dark brown to light brown. In the next step, it was mixed with 10 mL of ethyl acetate 3–4 times followed by dehydration with anhydrous sodium sulfate to get the desired pure product. Finally, the high spectroscopic techniques, i.e., ¹H and ¹³C NMR, were used for the determination of the novel derivatives' structures.

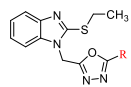
Biology. All compounds (15–35) of oxadiazole were evaluated for their AChE inhibitory activities in different concentrations. Majority of the oxadiazole compounds exhibit excellent inhibition, while few exhibit comparatively low inhibition. Compound 16 was the strongest inhibitor among all, with an IC₅₀ value of $41.87 \pm 0.67 \mu\text{M}$, which is comparable to the galanthamine IC₅₀ = $45.17 \pm 0.89 \mu\text{M}$. The inhibition of this compound may be due to the presence of the electron-donating octyl moiety. Ibrar *et al.* reported that in the coumarinyl oxadiazole series, a compound having an aliphatic group showed more potency against AChE as compared to aromatic substituents.²⁷ Compound 17 (IC₅₀ = $69.73 \pm 0.95 \mu\text{M}$) was the second potent compound of the series, which may be active due to the presence of a furan ring. Kamal *et al.* synthesize (*E*)-2-aryl-5-styryl-1,3, 4-oxadiazole derivatives and evaluate their potency against AChE. Among these analogues, 4g containing five-membered furan moiety at the carbon 2 position of the oxadiazole ring exhibited high inhibition in comparison with other compounds.¹⁴

Compounds 29 and 26 were the third most active inhibitors of AChE with IC₅₀ 84.17 ± 1.99 and $93.18 \pm 0.96 \mu\text{M}$, respectively. The potency of compound 29 may be attributed to the –F and –OCH₃ groups. It was previously reported that 1, 3, 4 oxadiazole compounds showed potency due to the presence of high electronegative groups such as –Cl and –F in

their structures.¹⁴ The activity of compound 26 was due to the hydroxyl moiety on the ortho position. Compound 22, having an IC₅₀ value of $97.94 \pm 0.79 \mu\text{M}$, showed inhibitory potential probably because of the existence of an alkylated furan ring, which makes it the fourth potent compound of the series. Compounds 23 and 15 with IC₅₀ values 117.99 ± 1.41 and $130.47 \mu\text{M}$ showed almost similar inhibitory activity. Inhibitions of these compounds may be due to halogen groups –Cl at a para position in compound 23 and –F at the ortho position in compound 15. It was previously suggested that the Cl group at the para position of the compound exhibited great potency against AChE.¹⁵ These compounds were more potent as compared to compound 25 (IC₅₀ = $208.29 \pm 1.39 \mu\text{M}$), having the same –Cl group at the ortho position. Compounds 31 and 32 with IC₅₀ values 248.46 ± 1.81 and $400.68 \pm 0.95 \mu\text{M}$ displayed anticholinesterase activity, which might be due to –OH groups. Compound 31 was more potent than compound 32, which may be due to the hydroxyl group on the para position, which is supported by the study of Mishra *et al.*¹⁵ They synthesized 4-aminopyridine tethered with substituted 1, 3, 4 oxadiazole derivatives; among these analogues, compound 9 with p-hydroxy substitution showed maximum inhibitory activity against hAChE.¹⁵ In the case of compounds 19 and 18, inhibition activities may be due to hydroxyl moieties, –OC₂H₅ and –OCH₃ groups, respectively. Compound 19 showed a better IC₅₀ ($223.52 \pm 0.96 \mu\text{M}$) value as compared to compound 18's IC₅₀ ($248.84 \pm 1.02 \mu\text{M}$) value probably due to the –OC₂H₅ group at the meta position. Compounds 21 and 20 with IC₅₀ values of 291.91 ± 0.87 and $380.06 \pm 0.87 \mu\text{M}$ showed their inhibition against AChE due to electron-donating –OCH₃ groups at different positions of the benzene ring. Compound 21 showed good inhibition as compared to compound 20, which may be due to the same –OCH₃ group at the para position. It was previously reported that the –OCH₃ group at the para position showed good inhibitory potential against AChE.¹⁵ Compound 35 exhibited inhibitory activity with IC₅₀ = $258.13 \pm 1.02 \mu\text{M}$; the activity of this compound might be due to the *N,N*-diethylaniline moiety. Compounds 33 and 34 showed better potency with IC₅₀ values of 320.64 ± 1.12 and $377.43 \pm 1.57 \mu\text{M}$, probably due to electron-donating groups –OH at the para and meta positions and in compound 33, the –CH₃ group at the ortho position of compound 34. Compounds 24, 28, 30, and 27 were less potent compounds of the series with IC₅₀ values 691.98 ± 0.99 , 750.86 ± 1.19 , 1189.98 ± 0.65 , and $1580.25 \pm 0.76 \mu\text{M}$, respectively (Table 1). In conclusion, the potency of most of the compounds in this series might be due to hydroxyl, halogens, amine, and alkyl groups.

Kinetics Studies of Inhibition of AChE by Oxadiazole (15–35). Enzyme kinetics is used to determine the inhibition mechanism of enzymes. In the present study, the inhibition mechanism was determined using linear Lineweaver–Burk plots. The substrate velocity curve in the presence and absence of the most active analogue (compound 16 for AChE) was recorded in the analysis of enzyme kinetics. The *K_i* values of compounds were investigated from the Lineweaver–Burk plot of the slope (*K_m*/*V_{max}*) versus varying concentrations.²⁸ The graphical representation of the steady-state inhibition of AChE is shown in Figure 1.

In the current study, it was found that all compounds (15–35) had good to moderate inhibitory activity against AChE. The IC₅₀ values of the compounds (15–35) were estimated at 41.87 ± 0.67 – $1580.25 \pm 0.76 \mu\text{M}$. As seen, compound 16

Table 1. Inhibitory Activity of Oxadiazole Derivatives (15–35) against AChE


Compound	R group	IC ₅₀ ±SEM (μM)	Docking Score
15		130.47±1.03	-11.944
16		41.87±0.67	-14.917
17		69.73±0.95	-13.366
18		248.84±1.02	-9.838
19		223.52±0.96	-10.487
20		380.06±0.87	-8.944
21		291.91±1.52	-9.199
22		97.94±0.79	-12.261
23		117.99±1.41	-12.155
24		691.98±0.99	-7.959
25		208.29±1.39	-11.007
26		93.18±0.96	-12.943
27		1580.25±0.76	-6.931
28		750.86±1.19	-7.561
29		84.17±1.99	-13.154
30		1189.98±0.65	-7.009
31		248.46±1.81	-10.880
32		400.68±0.95	-8.169
33		320.64±1.12	-8.917
34		377.43±1.57	-8.757
35		258.13±1.02	-9.284
Galanthamine		45.17±0.89	-12.394

(41.87 ± 0.67 μM) is the most potent inhibitor as compared to the remaining compounds 15 and 17–35. Accordingly, K_i of compound 16 (18.31 ± 1.7 μM) is lower as compared to the remaining compounds of the series, which showed its strong inhibitory potential against AChE as shown in Table 2.

Using the Lineweaver–Burk plot, various types of enzyme inhibition can be determined such as competitive, non-competitive, and mixed types. In the noncompetitive inhibitors' plot, same intersections occurred on the x -axis followed by different slopes and intersections on the y -axis as shown in Figure 2a. The current analysis pattern showed that all compounds of oxadiazole are noncompetitive inhibitors. These compounds interact with the enzyme–substrate complex or the free enzyme. Furthermore, the Lineweaver–Burk plot indicates that the tested compounds are reversible inhibitors as they bind to the AChE by noncovalent bonds including hydrogen, ionic, and hydrophobic interactions. These types of interactions are generated rapidly and can be removed easily. Therefore, enzyme kinetics have shown the biological significance of compound 16 and all other compounds due to their noncompetitive potential, contrasting irreversible inhibition where the complex is bound chemically and difficult to disjoin.

Confirmation of Screening Results based on the Protein–Ligand Interaction Fingerprint. Protein–ligand interaction fingerprint (PLIF) analyses were performed for validation of the molecular docking results. The PLIF descriptor is implemented in the MOE suit, which indicates efficiency of the primary interaction.²⁹ A database was created by using the docking procedure. Various interactions such as ionic, hydrogen bonding, and surface interactions were categorized as per residue, and a fingerprint scheme was generated that represents a database of the complex. All the docking confirmations were deposited to MOE PLIF, and the program was run with default parameters and a population plot was generated (Figure 2).

In the current study, all inhibitors were docked at the active site of 4EY6 to build the PLIF. Trp-86 was found to be the most important interacting residue with the active site of AChE followed by Phe-338, Tyr-124, Tyr-341, Ser-125, and His-447, as shown in Figure 2a,b.

Molecular Docking Results. Molecular docking was done to identify the most appropriate conformations of protein–ligand complexes. Docking studies sustain the *in vitro* study of the synthetic compounds and help determine the strength of the bonds by measuring bond lengths. Best interactions were selected based on low docking scores and strong binding interactions between inhibitor and receptor. In the current study, we docked all (15–35) compounds of the oxadiazole series in the pocket of AChE using MOE software. Few compounds having the best IC₅₀ and docking scores are discussed below.

From the docking conformation of compounds, it was shown that compound 16 (IC₅₀ = 41.87 ± 0.67 μM, docking score = -14.917) was the most potent compound of the series. Compound 16 established two π – π contacts with Trp-86 of the anionic subsite, and the oxadiazole ring of the same compound exhibited one arene–arene interaction with Tyr-341 of the Per-Arnt-Sim (PAS) subsite. Compound 16 N-moiety of the oxadiazole ring acts as an acceptor and formed one hydrogen bond with catalytic residue Tyr-124 with a bond length of 2.0 Å (Figure 3a,b). This compound showed good inhibitory potential as compared to galanthamine (IC₅₀ =

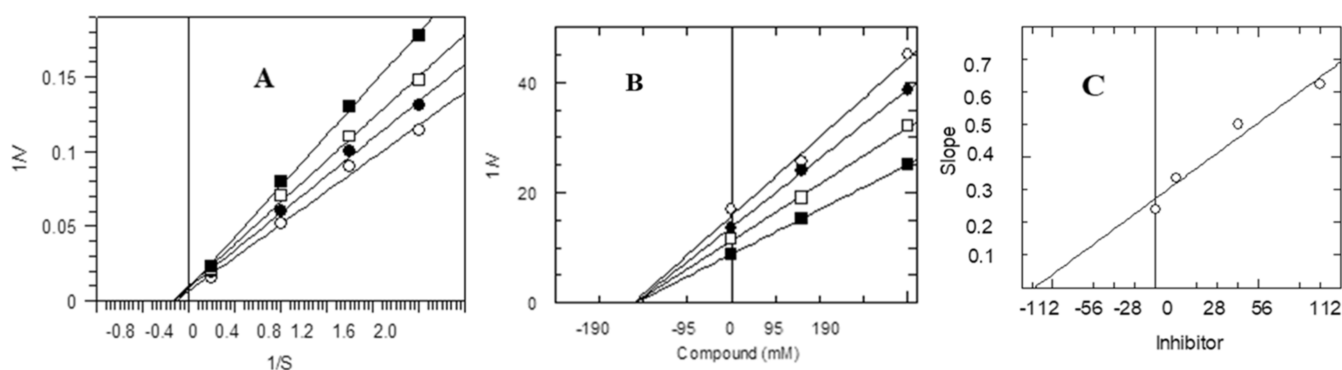


Figure 1. AChE inhibition by compound 16. (A) Lineweaver–Burk plot between four fixed ACh conc. in the absence (■) and presence of 100 μM (□), 150 μM (●), 175 μM (○) of compound 16. (B) Dixon plot of the reciprocal of the initial velocities and different concentrations of compound 16 at constant ACh concentrations (■) 100 μM , (□) 150 μM , (●) 175 μM , and (○) 200 μM . (C) Plot between different concentrations of compound 16 and slope.

Table 2. Inhibition of Kinetic Parameters Data of AChE in the Presence of Compounds (15–35)

compound	K_i (μM) \pm SEM	K_m (mM)	K_m (mM) <i>app</i>	V_{max} ($\mu\text{mol}/\text{min}$) ⁻¹	V_{maxapp}	type of inhibition
15	53.34 \pm 1.4	0.12	0.12	5.0	2.1	noncompetitive
16	18.31 \pm 1.7	0.12	0.12	5.0	2.3	noncompetitive
17	24.31 \pm 1.3	0.12	0.12	5.0	2.7	noncompetitive
18	98.77 \pm 0.7	0.12	0.12	5.0	2.5	noncompetitive
19	93.33 \pm 1.5	0.12	0.12	5.0	2.9	noncompetitive
20	147.3 \pm 1.9	0.12	0.12	5.0	2.3	noncompetitive
21	112.2 \pm 1.3	0.12	0.12	5.0	3.0	noncompetitive
22	32.11 \pm 1.4	0.12	0.12	5.0	3.0	noncompetitive
23	45.11 \pm 0.9	0.12	0.12	5.0	2.7	noncompetitive
24	284.17 \pm 1.2	0.12	0.12	5.0	2.4	noncompetitive
25	83.21 \pm 0.6	0.12	0.12	5.0	2.3	noncompetitive
26	30.49 \pm 1.9	0.12	0.12	5.0	2.5	noncompetitive
27	775.02 \pm 0.5	0.12	0.12	5.0	2.5	noncompetitive
28	289.22 \pm 0.8	0.12	0.12	5.0	2.2	noncompetitive
29	34.21 \pm 0.9	0.12	0.12	5.0	2.6	noncompetitive
30	456.71 \pm 0.2	0.12	0.12	5.0	2.5	noncompetitive
31	89.54 \pm 1.5	0.12	0.12	5.0	2.9	noncompetitive
32	148.81 \pm 0.2	0.12	0.12	5.0	2.5	noncompetitive
33	121.05 \pm 0.5	0.12	0.12	5.0	2.3	noncompetitive
34	135.16 \pm 0.5	0.12	0.12	5.0	2.4	noncompetitive
35	101.27 \pm 0.3	0.12	0.12	5.0	2.5	noncompetitive

45.17 \pm 0.89 μM , docking score = -12.394). Like compound 16, the same catalytic residues Try-124, Tyr-341, and Trp-86, except for Asp-74, were mainly involved in the galanthamine–AChE complex stabilization. Tyr-124 formed a strong H-bond with the methoxy group of galanthamine, having a bond length of 1.8 Å. Furthermore, the cyclohexanol ring of galanthamine acts as a donor and forms two hydrogen bonds with Asp-74 and Tyr-341 with the bond lengths of 2.8 and 2.9 Å, respectively. Trp-86 established one arene–cation interaction with the -NH group of a seven-membered ring of galanthamine (Figure 6a,b). Compound 16 had interactions mainly with PAS and anionic subsites and did not interact with the catalytic tract (His-447, Ser-203, Glu-334). Therefore, compound 16 showed noncompetitive inhibition. The kinetic analysis supports the docking results, which indicates that compound 16 has a noncompetitive mode of inhibition against AChE.

Molecular docking studies revealed that compound 17 is the second most potent compound with a docking score of -13.366 and IC_{50} value of 69.73 \pm 0.95 μM . This compound exhibited good inhibitory activity but was less potent as

compared to standard galanthamine, as shown in Table 1. Compound 17 is also less potent as compared to compound 16, which may be due to the large size and surface area interaction of compound 16 with the active site of AChE. The benzene ring of compound 17 formed two arene–arene interactions with Tyr-337 and Trp-86 as shown in Figure 4a,b. This compound formed interactions with only an anionic subsite and does not have interactions with catalytic triad and PAS. Consequently, our docking results are in agreement with the kinetic study, demonstrating a noncompetitive inhibition.

Compound 21 (IC_{50} = 84.17 \pm 1.99 μM , docking score = -13.154) is the third most active compound but less potent as compared to compounds 16 and 17 and standard galanthamine. Trp-86 of the anionic subsite molded the arene–arene interaction with the 1-fluoro-2-methoxybenzene moiety, while Tyr341 of PAS established the second arene–arene interaction with the imidazole ring of this compound as shown in Figure 5a,b. Our docking results indicate that all subsites of AChE are not involved in binding interactions. Therefore, docking analyses are in agreement with the kinetic measurements, showing a noncompetitive type of inhibition against AChE.

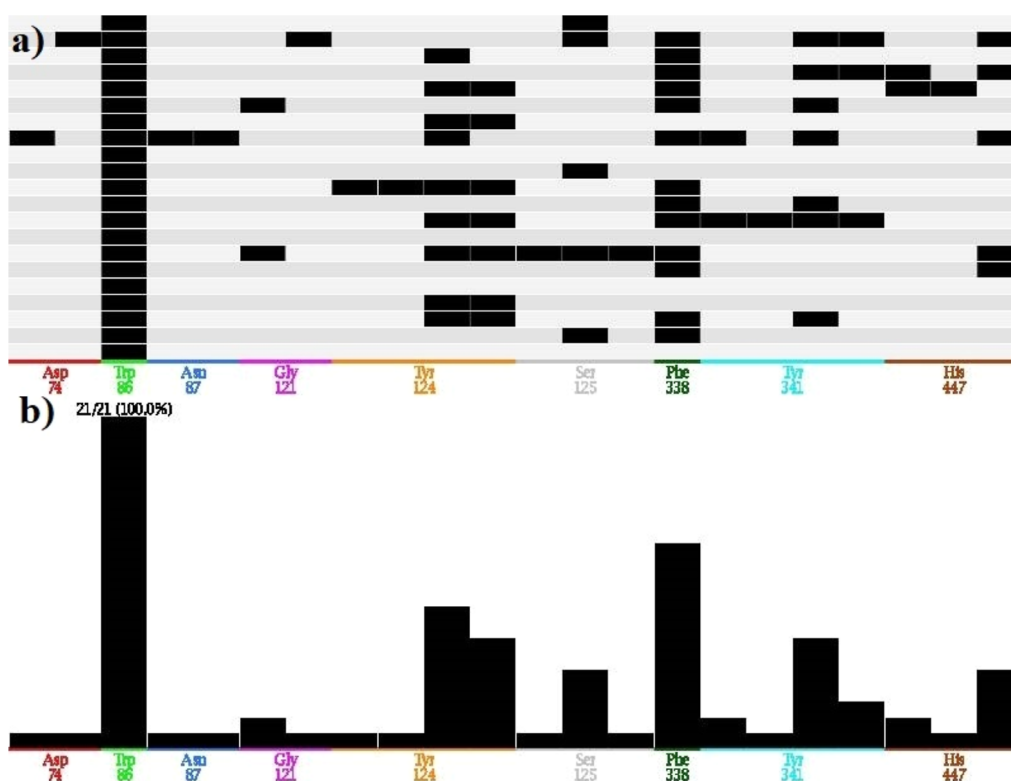


Figure 2. PLIF between potent inhibitors and the 4EY6 receptor [(a) barcodes, (b) populations].

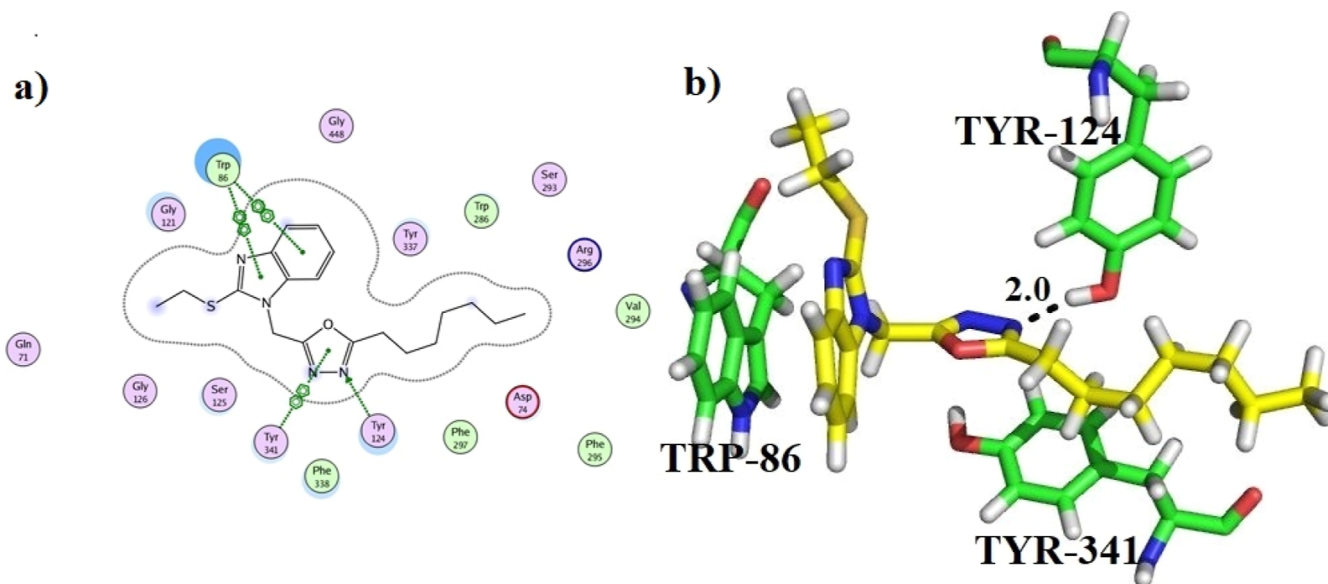


Figure 3. Docking conformation of compound 16 (a,b) in the active site of AChE.

Analysis of Molecular Dynamics Simulations. After docking, complexes were simulated for a total of 20 ns in an explicit water environment. The simulation of galanthamine with AChE has already been reported earlier [39]. Therefore, to check the stability of our complexes, root mean square deviation (RMSD) was calculated, which is a key parameter to determine the equilibrium of the MD trajectory of the backbone atoms of the protein chain throughout the MD simulation. Our results indicate that the RMSD curve of compound 16 in complex with AChE was initially unstable until 10 ns; afterward, it attained considerable stability up to 20

ns, as represented in Figure 7a. In the case of the compound 17–AChE complex, the RMSD curve was initially unstable, and high fluctuations were shown between 10 and 15 ns; the complex attains stability after 17 ns (Figure 7b). Our results revealed that the amplitude of RMSD for compound 16 in a complex with AChE is better in comparison to the stability of the compound 17–AChE complex.

The root mean square fluctuation (RMSF) shows the flexibility of each amino acid residue in the protein complexes. Our results revealed high fluctuations in the N-terminal, C-terminal, and loop regions. Additionally, the active site residues

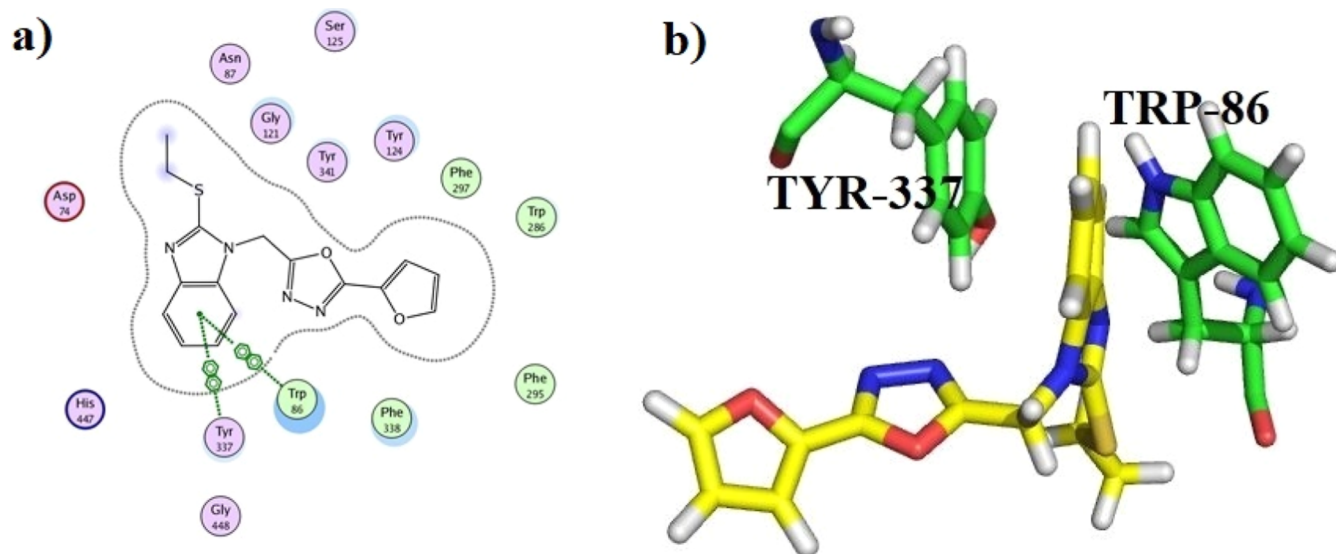


Figure 4. Docking conformation of compound 17 (a,b) in the active site of AChE.

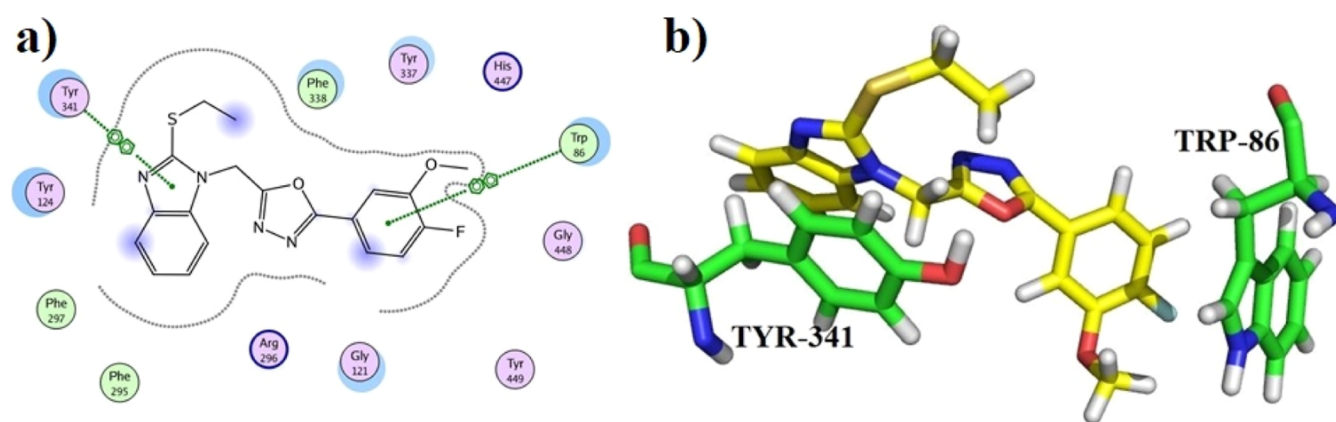


Figure 5. Docking pose of compound 21 (a,b) in the active site of AChE.

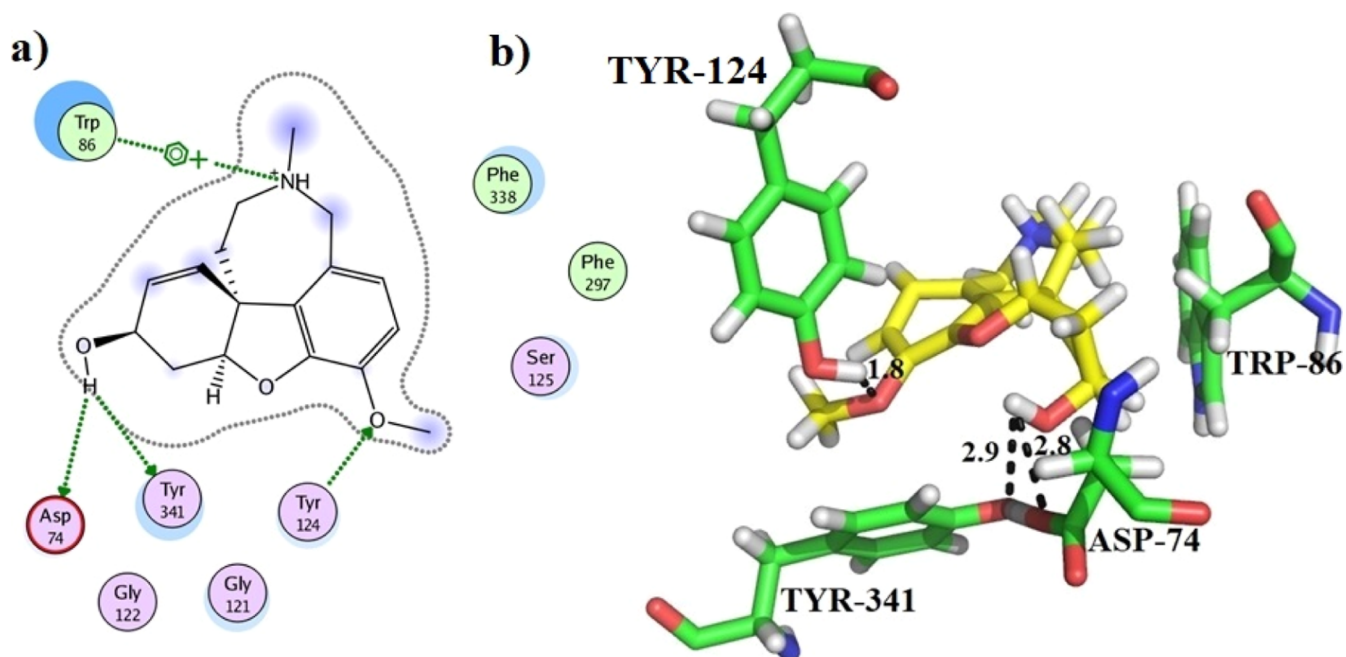


Figure 6. Docking conformation of galanthamine (a,b) (positive control) in the active site of AChE.

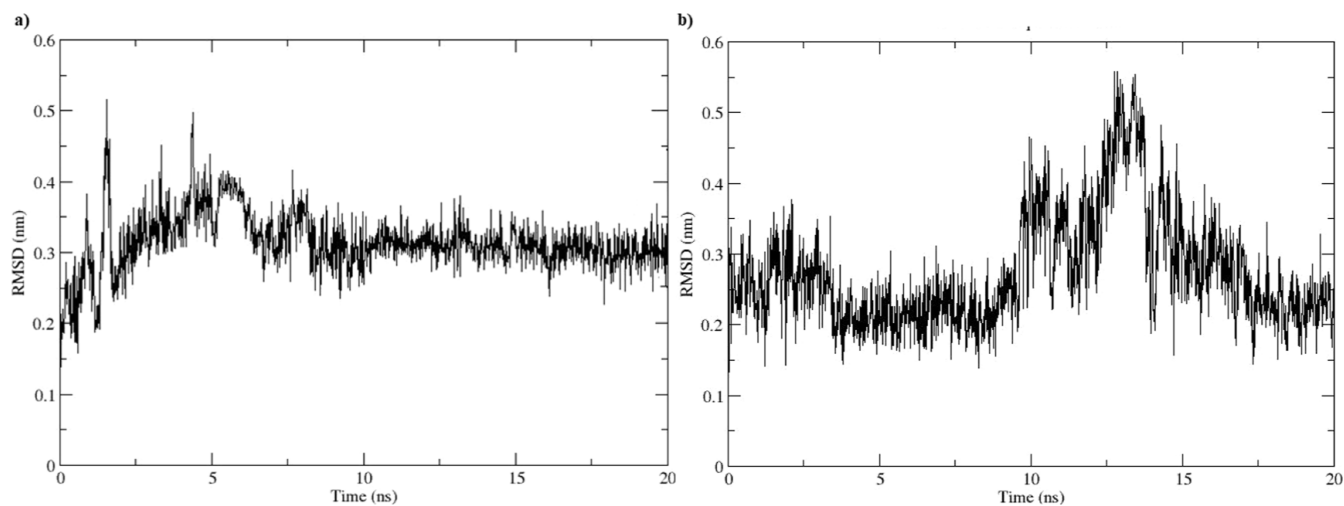


Figure 7. RMSD Plots for the (a) compound 16–AChE complex and (b) compound 17–AChE complex.

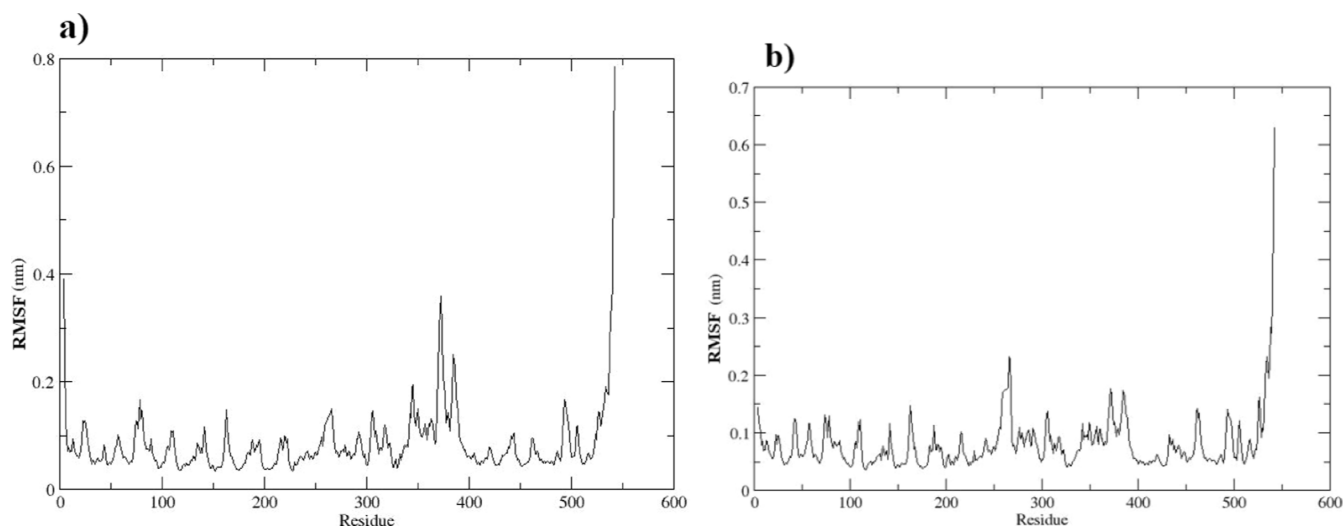


Figure 8. RMSF Plots for the (a) compound 16–AChE complex and (b) compound 17–AChE complex.

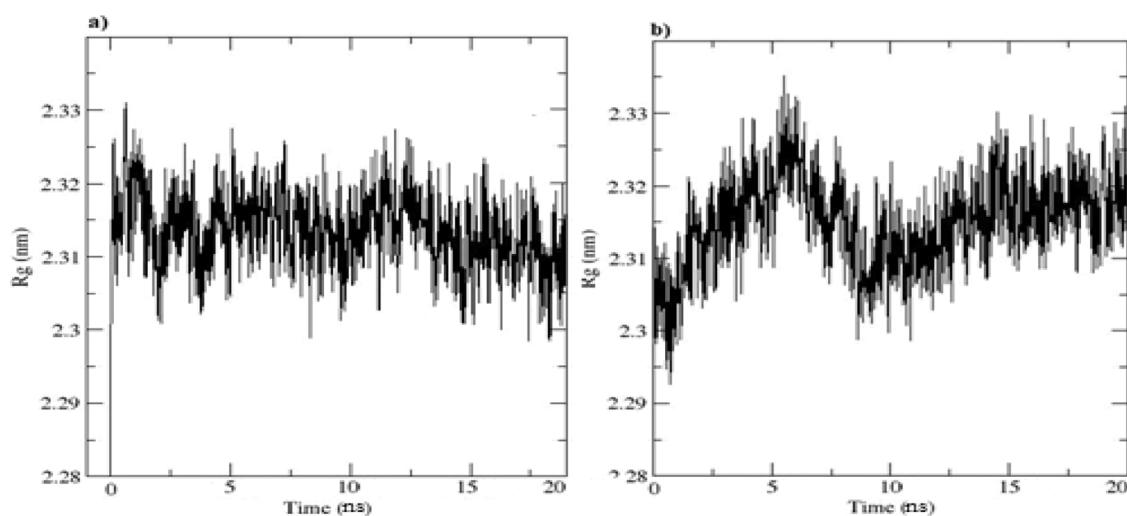


Figure 9. Rg Plots for the (a) compound 16–AChE complex and (b) compound 17–AChE complex.

and the residues forming secondary elements displayed lower RMSF values, *i.e.*, $> 2.5 \text{ \AA}$ (Figure 8a,b).

We further analyzed the compactness of the protein complex through the radius of the gyration parameter. Our results indicate that the compound 16–AChE complex remains highly

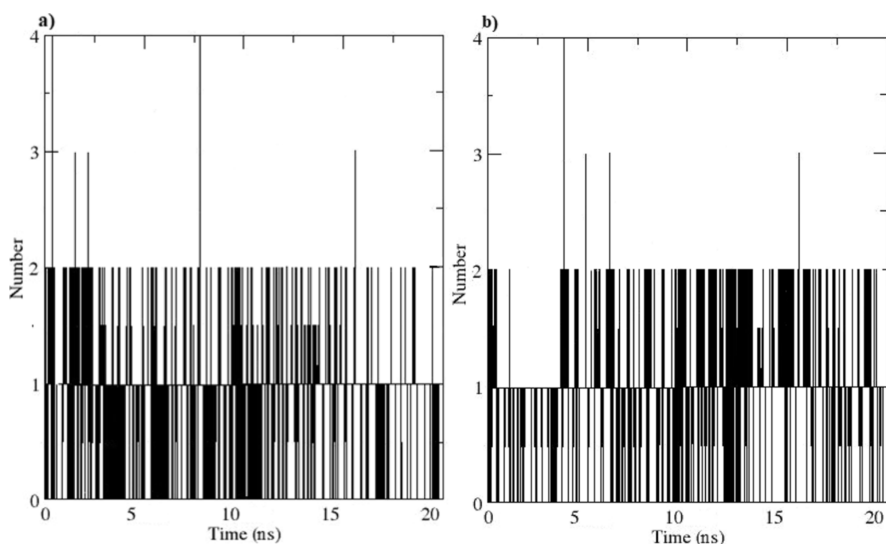


Figure 10. Hydrogen bonding for the (a) compound 16–AChE complex and (b) compound 17–AChE complex.

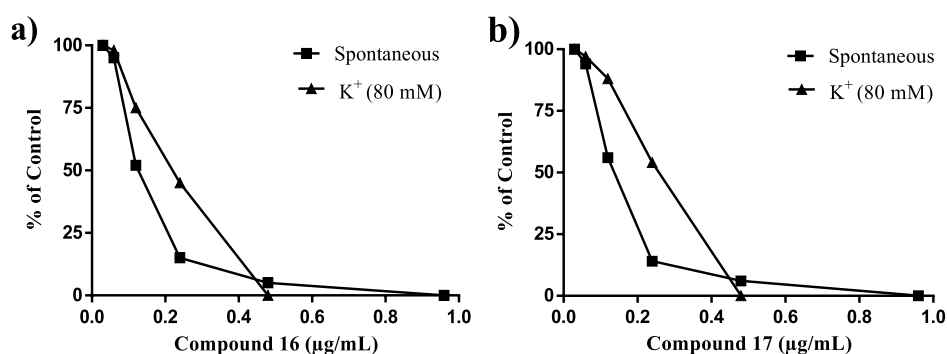


Figure 11. Dose–response curve presenting the spasmolytic effect of compound 16 (a) and 17 (b) on spontaneous and K^+ -induced contractions in rabbit jejunum (Mean \pm SEM, $n = 3$).

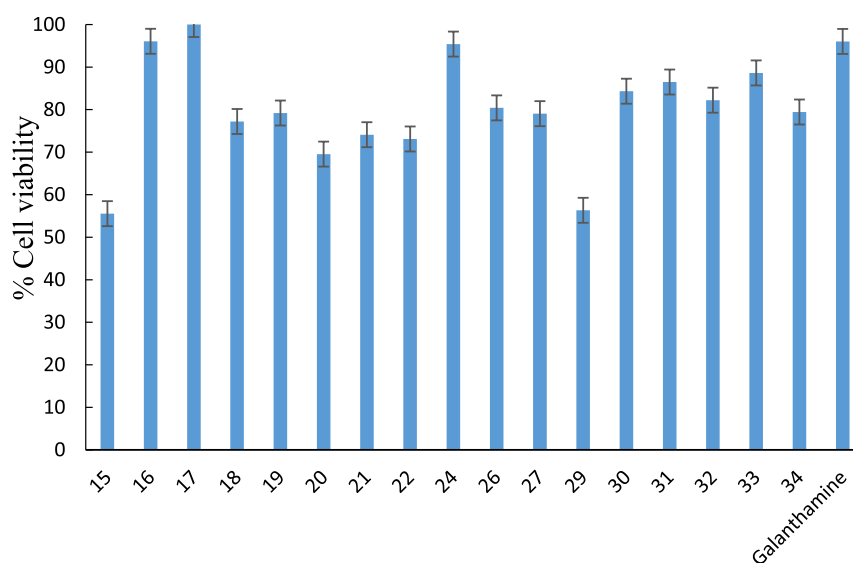


Figure 12. Bar graph representing the percentage of human neutrophil viability when treated with newly synthesized oxadiazole (15–35). Error bars are the standard deviations of triplicate experiments.

compact on ligand binding during the 20 ns MD simulation. However, for the compound 17–AChE complex, considerable fluctuations were observed in the R_g values until 13 ns, after which it attained significant compactness. Overall, lower

fluctuations were noticed in the R_g values of the compound 16–AChE complex in comparison to the compound 17–AChE complex, which reflects its better stability and compactness as shown in Figure 9a,b.

We also calculated the HB formation of these complexes throughout the 20 ns MD simulations. Our results show that both complexes retained almost similar HB interactions ranging from 0 to 4 during the 20 ns simulations, as shown in Figure 10a,b.

Antispasmodic and Calcium Antagonist Activities.

The movement of Ca^{2+} ions into the cytoplasm using voltage-gated Ca^{2+} channels causes spontaneous contraction, while the relaxant effects are caused by the Ca^{2+} removal from the cytoplasm.³⁰ In the current study, all compounds (15–35) showed the relaxation ability in a dose-dependent (0.003–1.0 $\mu\text{g}/\text{mL}$) manner to overcome the spontaneous and K^+ (80 mM)-induced contraction in rabbit jejunum (Table S1). Inhibition of the contraction may be due to the effect on entry and liberation of Ca^{2+} ions into the cytoplasm. Among the whole series of compounds, 16 and 17 were the most potent with median ED_{50} values of $0.12 \pm 0.00 \mu\text{g}/\text{mL}$, 0.22 ± 0.01 and 0.13 ± 0.07 , 0.26 ± 0.05 (Mean \pm SEM, $n = 3$) on spontaneous and K^+ -induced contractions, respectively (Figure 11). Our compounds were similar to verapamil, a standard Ca^{2+} channel antagonist inhibiting involuntary contraction. Furthermore, verapamil and another Ca^{2+} antagonist nifedipine are very effective in mental illness and AD treatment owing to the significant role of Ca^{2+} in controlling the activities of the brain.³¹ The Ca^{2+} hypothesis proclaimed that it prevents excess deposition of Ca^{2+} , mainly in damaged neurons. In AD, the cell loses its function, which may be due to the excess influx of Ca^{2+} that leads to cell death or neuronal dysfunction. By disturbing the equilibrium of the neurotransmitter and preventing excess intracellular Ca^{2+} levels,²⁷ oxadiazole double target direction agents (15–35) are likely to prolong cell survival and increase cell function.

Cytotoxicity Evaluation. Cytotoxic effects of the oxadiazole series (15–35) were found on human neutrophils by using standard operating protocol. FDA-approved drug galanthamine was utilized as the standard. Galanthamine is a widely used drug to treat AD. Human neutrophil viability at 200 $\mu\text{g}/\text{mL}$ concentrations of compounds 16, 17, and control galanthamine were found to be 96.07 ± 2.5 , 100.02 ± 1.0 , and $96.03 \pm 3.1\%$, respectively (Figure 12). These values indicate that compounds 16 and 17 are nontoxic. The minimum toxicity is the major advantage of the synthesized compounds. From the results (Table S2), it is clear that the remaining compounds are also nontoxic in nature as indicated by the neutrophil viability assay.

CONCLUSIONS

The current study helps to assess the underlying mechanisms of ligand and receptor interactions in this class of inhibitors. For this purpose, we performed kinetic studies, invitro AChE inhibitory assays, docking, and MD simulations. As a result, our compounds were found to be noncompetitive inhibitors against AChE and showed excellent to moderate activities with IC_{50} values of 41.87 ± 0.67 to $1580.25 \pm 0.76 \mu\text{M}$. Furthermore, these compounds have almost similar binding sites as they have similar structures to those of different functional groups. Compounds 16, 17, and 21 were the most active compounds of the series, and these complexes were stabilized by hydrogen bonding, are-arene interactions with Trp-86, Tyr-124, and Tyr-341 residues of anionic subsite, and PAS of the AChE. It is reported that beta aggregation is the early sign of AD, which can be prevented by noncompetitive inhibitors (drugs) that bind to the AChE PAS binding site.³²

The current study results indicate that some compounds are also noncompetitive inhibitors that interact with the PAS binding site of AChE. Therefore, we conclude that these compounds can be a suitable therapeutic option to prevent beta-aggregation in AD. Cytotoxicity was also determined by a cell base human neutrophil viability assay. Most of the AChE inhibitors were found to be nontoxic inhibitors and exhibited dose-dependent relaxation of muscle contraction, which makes them attractive drug candidates for new drug development.

ASSOCIATED CONTENT

Supporting Information

The Supporting Information is available free of charge at <https://pubs.acs.org/doi/10.1021/acsomega.3c06298>.

Superposition of a cocrystalline ligand conformation and docked confirmation; effective dose (ED_{50}) values of the compounds (15–35) for their spasmolytic effect; and viability test of human neutrophils (PDF)

AUTHOR INFORMATION

Corresponding Authors

Asaad Khalid – Substance Abuse and Toxicology Research Center, Jazan University, Jazan 45142, Saudi Arabia; Email: akahmed@jazanu.edu.sa

Ajmal Khan – Natural and Medical Sciences Research Centre, University of Nizwa, Nizwa 616, Sultanate of Oman; orcid.org/0000-0001-7851-6080; Email: ajmalchemist@yahoo.com

Muhammad Arif Lodhi – Department of Biochemistry, Abdul Wali Khan University Mardan, Khyber Pakhtunkhwa 23200, Pakistan; orcid.org/0000-0003-2120-884X; Email: arifbiochem@hotmail.com

Ahmed Al-Harrasi – Natural and Medical Sciences Research Centre, University of Nizwa, Nizwa 616, Sultanate of Oman; orcid.org/0000-0002-0815-5942; Email: aharrasi@unizwa.edu.com

Authors

Farida Begum – Department of Biochemistry, Abdul Wali Khan University Mardan, Khyber Pakhtunkhwa 23200, Pakistan

Muhammad Yousaf – Department of Chemistry, Government Post Graduate College Mardan, Khyber Pakhtunkhwa 23200, Pakistan

Sajid Iqbal – Atta-ur-Rahman School of Applied Biosciences (ASAB), National University of Sciences and Technology (NUST), Islamabad 44000, Pakistan

Nazif Ullah – Department of Biotechnology, Abdul Wali Khan University Mardan, Khyber Pakhtunkhwa 23200, Pakistan

Anwar Hussain – Department of Botany, Garden Campus, Abdul Wali Khan University Mardan, Khyber Pakhtunkhwa 23200, Pakistan

Momin Khan – Department of Chemistry, Abdul Wali Khan University Mardan, Khyber Pakhtunkhwa 23200, Pakistan; orcid.org/0000-0003-0936-5025

Alanood S. Algarni – Department of Pharmacology and Toxicology, College of Pharmacy, Umm Al-Qura University, Makkah 21955, Saudi Arabia

Ashraf N. Abdalla – Department of Pharmacology and Toxicology, College of Pharmacy, Umm Al-Qura University, Makkah 21955, Saudi Arabia; orcid.org/0000-0003-4770-9319

Complete contact information is available at:
<https://pubs.acs.org/10.1021/acsomega.3c06298>

Author Contributions

¹F.B. and M.Y. contributed equally. A.K., M.A.L., and F.B. designed the project. F.B. and S.I. performed the *in vitro* experiments and computational analysis. M.Y. and M.K. synthesized the compounds. F.B. and S.I. wrote the article. A.K., A.H., and N.U. reviewed and edited the manuscript. A.K., A.N.A., and A.S.A. achieved the funding acquisition. A.K., M.A.L., and A.A.-H. performed the supervision.

Notes

The authors declare no competing financial interest.

Ethics approval and consent to participate: The experimental procedures on animals were approved by the Institutional Ethical Committee of Abdul Wali Khan University Mardan (AWKUM) (ethical approval ID: AWKUM/pharm-19).

ACKNOWLEDGMENTS

The authors extend their appreciation to the Deputyship for Research and Innovation, Ministry of Education in Saudi Arabia for funding this research work through the project number (ISP23-81).

REFERENCES

- (1) Hugo, J.; Ganguli, M. Dementia and cognitive impairment: epidemiology, diagnosis, and treatment. *Clin. Geriatr. Med.* **2014**, *30* (3), 421–442.
- (2) Piplani, P.; Jain, A.; Devi, D.; Anjali; Sharma, A.; Silakari, P. Design, synthesis and pharmacological evaluation of some novel indanone derivatives as acetylcholinesterase inhibitors for the management of cognitive dysfunction. *Bioorg. Med. Chem.* **2018**, *26* (1), 215–224.
- (3) Sosa-Ortiz, A. L.; Acosta-Castillo, I.; Prince, M. J. Epidemiology of dementias and Alzheimer's disease. *Arch. Med. Res.* **2012**, *43* (8), 600–608.
- (4) Association, A. s.. 2012 Alzheimer's disease facts and figures. *Alzheimer's & Dementia*, 2012; Vol. 8, pp 131–168.2.
- (5) (a) Folch, J.; Petrov, D.; Ettcheto, M.; Abad, S.; Sánchez-López, E.; García, M. L.; Olloquequi, J.; Beas-Zarate, C.; Auladell, C.; Camins, A. Current research therapeutic strategies for Alzheimer's disease treatment. *Neural Plast.* **2016**, *2016*, 1–15. (b) Godyń, J.; Jończyk, J.; Panek, D.; Malawska, B. Therapeutic strategies for Alzheimer's disease in clinical trials. *Pharmacol. Rep.* **2016**, *68* (1), 127–138.
- (6) (a) Lemes, L. F. N.; de Andrade Ramos, G.; de Oliveira, A. S.; da Silva, F. M. R.; de Castro Couto, G.; da Silva Boni, M.; Guimarães, M. J. R.; Souza, I. N. O.; Bartolini, M.; Andrisano, V.; et al. Cardanol-derived AChE inhibitors: Towards the development of dual binding derivatives for Alzheimer's disease. *Eur. J. Med. Chem.* **2016**, *108*, 687–700. (b) Kumar, A.; Nisha, C. M.; Silakari, C.; Sharma, I.; Anusha, K.; Gupta, N.; Nair, P.; Tripathi, T.; Kumar, A. Current and novel therapeutic molecules and targets in Alzheimer's disease. *J. Formos. Med. Assoc.* **2016**, *115* (1), 3–10. (c) Srivastava, P.; Tripathi, P. N.; Sharma, P.; Rai, S. N.; Singh, S. P.; Srivastava, R. K.; Shankar, S.; Shrivastava, S. K. Design and development of some phenyl benzoxazole derivatives as a potent acetylcholinesterase inhibitor with antioxidant property to enhance learning and memory. *Eur. J. Med. Chem.* **2019**, *163*, 116–135.
- (7) (a) Shrivastava, S. K.; Sinha, S. K.; Srivastava, P.; Tripathi, P. N.; Sharma, P.; Tripathi, M. K.; Tripathi, A.; Choubey, P. K.; Waiker, D. K.; Aggarwal, L. M.; et al. Design and development of novel p-aminobenzoic acid derivatives as potential cholinesterase inhibitors for the treatment of Alzheimer's disease. *Bioorg. Chem.* **2019**, *82*, 211–223. (b) Sinha, S. K.; Shrivastava, S. K. Synthesis and evaluation of some new 4-aminopyridine derivatives as a potent anti-amnesic and

cognition enhancing drugs. *Med. Chem. Res.* **2012**, *21*, 4395–4402. (c) Sinha, S. K.; Shrivastava, S. K. Synthesis, evaluation and molecular dynamics study of some new 4-aminopyridine semicarbazones as an anti-amnesic and cognition enhancing agents. *Bioorg. Med. Chem.* **2013**, *21* (17), 5451–5460.

(8) (a) Tripathi, P. N.; Srivastava, P.; Sharma, P.; Tripathi, M. K.; Seth, A.; Tripathi, A.; Rai, S. N.; Singh, S. P.; Shrivastava, S. K. Biphenyl-3-oxo-1, 2, 4-triazine linked piperazine derivatives as potential cholinesterase inhibitors with anti-oxidant property to improve the learning and memory. *Bioorg. Chem.* **2019**, *85*, 82–96. (b) Sharma, P.; Srivastava, P.; Seth, A.; Tripathi, P. N.; Banerjee, A. G.; Shrivastava, S. K. Comprehensive review of mechanisms of pathogenesis involved in Alzheimer's disease and potential therapeutic strategies. *Prog. Neurobiol.* **2019**, *174*, 53–89.

(9) Bartolini, M.; Bertucci, C.; Cavrini, V.; Andrisano, V. β -Amyloid aggregation induced by human acetylcholinesterase: inhibition studies. *Biochem. Pharmacol.* **2003**, *65* (3), 407–416.

(10) (a) Sharma, P.; Tripathi, A.; Tripathi, P. N.; Prajapati, S. K.; Seth, A.; Tripathi, M. K.; Srivastava, P.; Tiwari, V.; Krishnamurthy, S.; Shrivastava, S. K. Design and development of multitarget-directed N-Benzylpiperidine analogs as potential candidates for the treatment of Alzheimer's disease. *Eur. J. Med. Chem.* **2019**, *167*, 510–524. (b) Tripathi, P. N.; Srivastava, P.; Sharma, P.; Seth, A.; Shrivastava, S. K. Design and development of novel N-(pyrimidin-2-yl)-1, 3, 4-oxadiazole hybrids to treat cognitive dysfunctions. *Bioorg. Med. Chem.* **2019**, *27* (7), 1327–1340.

(11) Mao, P.; Reddy, P. H. Aging and amyloid beta-induced oxidative DNA damage and mitochondrial dysfunction in Alzheimer's disease: implications for early intervention and therapeutics. *Biochim. Biophys. Acta (BBA)—Mol. Basis Dis.* **2011**, *1812* (11), 1359–1370.

(12) (a) Rehman, A.-u.; Nafeesa, K.; Abbasi, M. A.; Siddiqui, S. Z.; Rasool, S.; Shah, S. A. A.; Ashraf, M. Synthesis of new heterocyclic 3-piperidiny-1, 3, 4-oxadiazole derivatives as potential drug candidate for the treatment of Alzheimer's disease. *Cogent Chem.* **2018**, *4* (1), 1472197. (b) Mei, W.-w.; Ji, S.-s.; Xiao, W.; Wang, X.-d.; Jiang, C.-s.; Ma, W.-q.; Zhang, H.-y.; Gong, J.-x.; Guo, Y.-w. Synthesis and biological evaluation of benzothiazol-based 1, 3, 4-oxadiazole derivatives as amyloid β -targeted compounds against Alzheimer's disease. *Monatshfte für Chemie-Chemical Monthly* **2017**, *148*, 1807–1815.

(13) Rehman, A.; Fatima, A.; Abbas, N.; Abbasi, M. A.; Khan, K. M.; Ashraf, M.; Ahmad, I.; Ejaz, S. A. Synthesis, characterization and biological screening of 5-substituted-1, 3, 4-oxadiazole-2-yl-N-(2-methoxy-5-chlorophenyl)-2-sulfanyl acetamide. *Pak. J. Pharm. Sci.* **2013**, *26* (2), 345–352.

(14) Kamal, A.; Shaik, A. B.; Reddy, G. N.; Kumar, C. G.; Joseph, J.; Kumar, G. B.; Purushotham, U.; Sastry, G. N. Synthesis, biological evaluation, and molecular modeling of (E)-2-aryl-5-styryl-1, 3, 4-oxadiazole derivatives as acetylcholine esterase inhibitors. *Med. Chem. Res.* **2014**, *23*, 2080–2092.

(15) Mishra, P.; Sharma, P.; Tripathi, P. N.; Gupta, S. K.; Srivastava, P.; Seth, A.; Tripathi, A.; Krishnamurthy, S.; Shrivastava, S. K. Design and development of 1, 3, 4-oxadiazole derivatives as potential inhibitors of acetylcholinesterase to ameliorate scopolamine-induced cognitive dysfunctions. *Bioorg. Chem.* **2019**, *89*, 103025.

(16) Hasan, A.; Khan, K. M.; Sher, M.; Maharvi, G. M.; Nawaz, S. A.; Choudhary, M.; Atta-ur-Rahman; Supuran, C. T. Synthesis and inhibitory potential towards acetylcholinesterase, butyrylcholinesterase and lipoxigenase of some variably substituted chalcones. *J. Enzym. Inhib. Med. Chem.* **2005**, *20* (1), 41–47.

(17) Khan, F. A.; Shamim, S.; Ullah, N.; Lodhi, M. A.; Khan, K. M.; Kanwal; Ali, F.; Ali, F.; Afridi, S. G.; Perveen, S.; Khan, A. Dihydropyrimidones: A ligands urease recognition study and mechanistic insight through in vitro and in silico approach. *Med. Chem. Res.* **2021**, *30*, 120–132.

(18) Leatherbarrow, R. J. *GraFit user's guide*; Ertihacus Software Ltd, 1992.

(19) Martínez-Rosell, G.; Giorgino, T.; De Fabritiis, G. Play-Molecule ProteinPrepare: a web application for protein preparation

for molecular dynamics simulations. *J. Chem. Inf. Model.* **2017**, *57* (7), 1511–1516.

(20) Van Der Spoel, D.; Lindahl, E.; Hess, B.; Groenhof, G.; Mark, A. E.; Berendsen, H. J. GROMACS: fast, flexible, and free. *J. Comput. Chem.* **2005**, *26* (16), 1701–1718.

(21) Berendsen, H. J.; van der Spoel, D.; van Drunen, R. GROMACS: A message-passing parallel molecular dynamics implementation. *Comput. Phys. Commun.* **1995**, *91* (1–3), 43–56.

(22) Nath, O.; Singh, A.; Singh, I. K. In-Silico Drug discovery approach targeting receptor tyrosine kinase-like orphan receptor 1 for cancer treatment. *Sci. Rep.* **2017**, *7* (1), 1029.

(23) Yang, B.; Lin, S.-J.; Ren, J.-Y.; Liu, T.; Wang, Y.-M.; Li, C.-M.; Xu, W.-W.; He, Y.-W.; Zheng, W.-H.; Zhao, J.; et al. Molecular docking and molecular dynamics (MD) simulation of human anti-complement factor H (CFH) antibody Ab42 and CFH polypeptide. *Int. J. Mol. Sci.* **2019**, *20* (10), 2568.

(24) Hess, B.; Bekker, H.; Berendsen, H. J.; Fraaije, J. G. LINCS: A linear constraint solver for molecular simulations. *J. Comput. Chem.* **1997**, *18* (12), 1463–1472.

(25) Petersen, H. G. Accuracy and efficiency of the particle mesh Ewald method. *J. Chem. Phys.* **1995**, *103* (9), 3668–3679.

(26) Gilani, A. H.; Janbaz, K.; Zaman, M.; Lateef, A.; Tariq, S.; Ahmad, H. Hypotensive and spasmolytic activities of crude extract of *Cyperus scariosus*. *Arch. Pharmacol. Res.* **1994**, *17*, 145–149.

(27) Ibrar, A.; Khan, A.; Ali, M.; Sarwar, R.; Mehsud, S.; Farooq, U.; Halimi, S. M.; Khan, I.; Al-Harrasi, A. Combined in vitro and in silico studies for the anticholinesterase activity and pharmacokinetics of coumarinyl thiazoles and oxadiazoles. *Front. Chem.* **2018**, *6*, 61.

(28) Can, Ö. D.; Osmaniye, D.; Demir Özkay, Ü.; Sağlık, B. N.; Levent, S.; Iğın, S.; Baysal, M.; Özkay, Y.; Kaplancikli, Z. A. MAO enzymes inhibitory activity of new benzimidazole derivatives including hydrazone and propargyl side chains. *Eur. J. Med. Chem.* **2017**, *131*, 92–106.

(29) Liang, J.-w.; Zhang, T.-j.; Li, Z.-j.; Chen, Z.-x.; Yan, X.-l.; Meng, F.-h. Predicting potential antitumor targets of Aconitum alkaloids by molecular docking and protein–ligand interaction fingerprint. *Med. Chem. Res.* **2016**, *25*, 1115–1124.

(30) (a) Rivera, L.; Brading, A. F. The role of Ca²⁺ influx and intracellular Ca²⁺ release in the muscarinic-mediated contraction of mammalian urinary bladder smooth muscle. *BJU Int.* **2006**, *98* (4), 868–875. (b) Voussen, B.; Beck, K.; Mauro, N.; Keppler, J.; Friebe, A. Comparison of nitrenergic signaling in circular and longitudinal smooth muscle of murine ileum. *Neurogastroenterol. Motil.* **2018**, *30* (3), No. e13175. (c) Montgomery, L. E.; Tansey, E. A.; Johnson, C. D.; Roe, S. M.; Quinn, J. G. Autonomic modification of intestinal smooth muscle contractility. *Adv. Physiol. Educ.* **2016**, *40* (1), 104–109.

(31) Vagnucci, A. H.; Li, W. W. Alzheimer's disease and angiogenesis. *Lancet* **2003**, *361* (9357), 605–608.

(32) Choudhary, M. I.; Nawaz, S. A.; ul-Haq, Z.; Lodhi, M. A.; Ghayur, M. N.; Jalil, S.; Riaz, N.; Yousuf, S.; Malik, A.; Gilani, A. H.; et al. Withanolides, a new class of natural cholinesterase inhibitors with calcium antagonistic properties. *Biochem. Biophys. Res. Commun.* **2005**, *334* (1), 276–287.

NOTE ADDED AFTER ASAP PUBLICATION

This article originally published with an error in an author name and Figure 12. Nazif Ullah's name and Figure 12 were corrected and the article reposted November 29, 2023.